Journal of Applied Biology & Biotechnology Vol. 11(6), pp. 233-248, Nov-Dec, 2023
Available online at http://www.jabonline.in
DOI: 10.7324/JABB.2023.115277

Characterization and comparative assessment of bactericidal activity of carbon nanodots (CDs) and nanoparticles (CNPs) prepared from soot's of clarified butter and mustard oil, respectively

Vikas Pahal[1*], Pankaj Kumar[2], Rahul Kumar[1], Parveen Kumar[3], Vinod Kumar[4]

[1]Department of Microbiology, Dolphin PG College of Science and Agriculture, Chunni Kalan, Fatehgarh Sahib, Punjab, India.
[2]Department of Microbiology, Dolphin PG Institute of Biomedical and Natural Sciences, Dehradun, Uttrakhand, India.
[3]Bio-Nanotechnology Lab, Central Scientific Instruments Organization, Chandigarh, India.
[4]HR-TEM Facility Lab, Department of pharmacology and toxicology, National Institute of Pharmaceutical Education and Research (NIPER), SAS Nagar, Mohali, Punjab, India.

ARTICLE INFO

Article history:
Received on: January 25, 2023
Accepted on: July 18, 2023
Available online: October 25, 2023

Key words:
Carbon nanodots, carbon nanospheres, bactericidal effect, XTT-colorimetric assay

ABSTRACT

Carbon nanoparticles (CNPs) are carbon-based nanomaterial with dimensions in the range of 1–100 nm. In the present research, an ecofriendly, simple, and highly reproducible method was used to prepare the CNPs from the soot of clarified butter (carbon dots) and mustard oil (carbon nanospheres) in both pristine and oxidized forms. The obtained CNPs were subjected to various analyses such as UV-visible, Fourier transform infrared (FTIR), dynamic light scattering, high-resolution transmission electron microscopy, energy-dispersive X-ray, and X-ray diffraction (XRD). The analyses demonstrate that the size of butter-originated CNPs was found in the ranges of 10–90 nm (raw) and 5–20 nm (oxidized), whereas, in the case of mustard oil-originated CNPs, the size was observed in the ranges of 100–150 nm (raw) and 50–80 nm (oxidized). As per zeta potential results, the net surface charges on CNPs were observed as −9.05 and −14.6 mV in the case of raw and oxidized CNPs from butter, respectively, and −12.7 and −20.1 mV in the case of raw and oxidized CNPs from mustard oil, respectively. XRD results showed the typical graphitic crystalline nature of both kinds of CNPs irrespective of their initial raw material. FTIR results confirmed hydroxyl, carboxyl, carbonyl, and amide groups on CNPs that help in their capping and stabilization in the solvent media. Five bacterial strains, *Staphylococcus aureus*, *Escherichia coli*, *Staphylococcus epidermidis*, *Klebsiella pneumoniae*, and *Moraxella catarrhalis*, were used to assess the bactericidal potential of synthesized CNPs using agar-well and 2,3-bis-(2-methoxy-4-nitro-5-sulfophenyl)-2*H*-tetrazolium-5-carboxanilide-colorimetric methods. Butter-mediated oxidized CNPs were the most effective bactericidal agent against all the bacterial strains compared to mustard-originated CNPs. Furthermore, CNPs-mediated toxicity towards bacteria was both size and concentration dependent. *Staphylococcus aureus* and *S. epidermidis* were the most sensitive [minimum inhibitory concentration (MIC): 800 µg/ml] and resistant (MIC: 2.0 mg/ml) bacteria, respectively, towards CNPs-mediated toxicity. The synthesized CNPs were devoid of any metallic impurities and hence worthy of being used in various applications like imaging, labeling, sensor-technology, and environment monitoring and as an antibacterial agent.

1. INTRODUCTION

Carbon, the most abundant and essential building element of life, has been enthralling scientists for ages. In recent decades, carbon-based nanometer-sized allotropes like carbon nanotubes (CNTs), Carbon nanoparticles (CNPs), carbon nanodots (CDs), carbon nanofibers, graphene/graphite nanosheets, fullerene, nanorods, nanodiamonds, nano-onions, and other such structures are mesmerizing scientists because of their great importance and applications in diversified fields [1–3]. These carbon-based nanostructures possess exceptional physicochemical and electrochemical properties such as optical properties, magnetic properties, catalytic properties, thermal stability, mechanical properties, biocompatibility, resistance to degradation, presence of large reactive surface area per unit volume, electrical conductivity, excellent adsorption characteristics, easiness in surface modifications, and ideal drug delivery property. These

*Corresponding Author
Dr. Vikas Pahal, Department of Microbiology, Dolphin PG College of Science and Agriculture, Chunni Kalan, Fatehgarh Sahib, Punjab, India.
E-mail: vikaspahal3 @ gmail.com

remarkable properties make them useful in various industrial and commercial applications [1,3–6]. Recently, these carbon-based nanomaterials, especially CDs (size <10 nm) and carbon nanospheres (size: 10–90 nm), have been found to have promising applications in the environment, medical, and pharma industries as an excellent material for biosensing and bioimaging [7,8], drug delivery, protective coatings, and antimicrobial/biocidal agents [9,10], wavelength-pitched color production [11], nano- and aptasensors [7,8,12], pollutant removing material, ultrasensitive fluorescent imaging, and immunoassays [13–16], sequencing of nucleic acids, bioseparation, probes, and biocatalysis [17,18], and other biomedical applications [19].

Irrational and overuse of antibacterial drugs resulted in the evolution of multiple drug-resistant bacterial strains, which further leads to several consequences, including the enhanced mortality and morbidity rate [20,21], inefficiency of antibiotics or other therapeutic drugs, and expensive treatment strategies which directly increases the financial burden for any country [21,22]. This problem encourages researchers throughout the world to synthesize and develop novel and low-cost antibacterial agents of the next generation, which have high bactericidal effects with low to negligible side effects on the human body. In the last couple of decades, various inorganic NPs (like gold, silver, zinc, titanium, copper, iron, etc.) were developed and assessed for their bactericidal properties. These inorganic NPs were found to have potential bactericidal properties, but the problem remains with their adverse toxic and immunogenic side effects on human cells and tissues**.** As carbon is the basic building block of life and also the most biocompatible, nonimmunogenic, chemically inert, and nontoxic to the human body with good cell permeability, a great interest has arisen in the synthesis of various carbon nanomaterials of different shapes and sizes as bactericidal agents from natural sources [11,15]. A perusal of literature demonstrated that activated CNPs could be synthesized from various carbon source materials like cooking oil, rice bran, curcumin, coconut shell, kitchen soot, candle soot, fruits juice, and sugarcane bagasse [11,15] using different physical, chemical, and hybrid approaches including chemical oxidation, electrochemical oxidation, laser ablation, microwave irradiation, combustion/hydrothermal approach, carbonization, pyrolysis, chemical vapor deposition method, sono-chemical approach, and electric arc discharge method [1,3,8,11,23–25]. These synthesis and isolation methods of activated CNPs from biowaste materials have been getting significant attention since the last decade due to their easy availability, low-cost production, ecofriendly nature, and abundance of precursor materials. In the present research, a highly reproducible, ecofriendly, and easy method was used to synthesize CNPs from the soot of mustard oil (*Brassica campestris*) and clarified butter of indigenous white cow (*Bos indicus*), and their physical attributes were analyzed using various physical techniques. As per the Ayurveda system of medicine and also in traditional knowledge, cow's clarified butter (also called "ghee") and mustard oil both possess antibacterial, antifungal, antioxidant, and antiviral properties [26–31]. There is scanty information in the literature regarding the bactericidal potency of carbon dots and carbon nanospheres, and those which are available have been based only on agar-well diffusion results. The agar-well diffusion method has certain limitations [32], like hindrance of CNPs free movement in solid agar, less area of contact between CNPs and bacteria, etc. To avoid these limitations and for more authentic results of CNPs' bactericidal potential, we used the gold standard 2,3-bis-(2-methoxy- 4-nitro-5-sulfophenyl)-2H-tetrazolium-5-carboxanilide (XTT)-colorimetric method, a liquid-media-based method [33–35]. The present research objective was twofold: to have a cost-effective and reproducible method of production of CDs and carbon nanospheres from natural resources and second to get authentic results of their bactericidal efficiency against diverse kinds of pathogenic bacterial strains.

2. MATERIALS AND METHODS

2.1. Chemicals and Raw Materials for Synthesis of CNPs

Pure mustard oil (*B. campestris*) and butter of indigenous white cow (*B. indicus*) were procured from the local market, Chunni Kalan, Fatehgarh Sahib, Punjab. The Mueller-Hinton agar (MHA) and broth (MHB), sodium-phosphate buffer, nitric acid (HNO_3), acetone (CH_3COCH_3), chloroform ($CHCl_3$), ethanol (CH_3CH_2OH), and high performance liquid chromatography (HPLC) purified water were purchased from HiMedia Pvt. Ltd., Chandigarh (UT), India. The sodium salt of XTT and menadione were purchased from Sigma-Aldrich, Chandigarh (UT), India.

2.2. Preparations of Raw/Pristine CNPs

CNPs were prepared from oil and butter using the lamp-soot method with some modifications [36]. In this method, both the oil and butter were placed in a separate reservoir (100 ml glass beaker) containing a nonabsorbent cotton wick. A tip of the cotton wick was ignited, and the soot was collected on the inverted receiver glass beaker, which was kept above the reservoir beaker in a laminar air-flow chamber. After complete oil and ghee burning, carbon particles were scratched by a spatula and collected in a sterilized glass bottle. The extracted soot (100 mg) was dissolved in a mixture of ethanol, water, and chloroform (3:1:1 v/v ratio, respectively) using a magnetic stirrer for 10–12 hours at temperature 45°C + 2°C, followed by centrifugation at 8,000 rpm for 10–12 minutes. This step was repeated thrice, and the heavy residue which settled down was discarded. The supernatant was collected in a new tube and again centrifuged at 16,000 rpm for 20–25 minutes. CNPs in the form of pellets obtained by this method were further washed thrice with ethanol and dried in a vacuum oven at 50°C–55°C for 2–3 hours and were labeled as mustard oil mediated raw carbon nanoparticles (MCR) and butter mediated raw carbon nanoparticles (BCR) for the CNPs obtained from oil and butter, respectively.

2.3. Preparation of Oxidized Form of CNPs

100 mg of carbon powder material (collected from the burning lamp) was dissolved in 200 ml of 2.5 M nitric acid (HNO_3) and refluxed at 90°C–95°C for 24 hours on a magnetic stirrer followed by cooling at room temperature. After that, the solution was centrifuged for 10 minutes at 8,000 rpm to get rid of the unreacted carbon soot, which was settled down as a pellet. After centrifugation, the supernatant became yellow-brownish in color, which indicates the presence of water-soluble CNPs in the solution. The yellow-brownish supernatant thus obtained was mixed with an equal volume of acetone and water solvent (3:1 v/v ratio, respectively) and vigorously shaken. The mixed supernatant was then centrifuged for 15–20 minutes at 16,000 rpm. The pellets were

collected, and this step of purification was repeated thrice to remove excess nitric acid from the CNPs. After purification, the pellets were resuspended in ethanol/HPLC purified water (volume ratio 1:1) and again centrifuged at 16,000 rpm for 15–20 minutes. At last, CNPs were dried in a vacuum oven at 50°C–55°C for 2–3 hours. The obtained CNPs from oil and butter by this method were labeled as mustard oil mediated oxidized carbon nanoparticles (MCO) and butter mediated oxidized carbon nanopartic (BCO), respectively.

2.4. Characterization of CNPs

The prepared CNPs were characterized by using various biophysical techniques like UV-vis spectroscopy, high-resolution transmission electron microscopy (HRTEM), dynamic light scattering (DLS), zeta potential, Fourier transform infrared (FTIR) spectroscopy, X-ray diffraction (XRD), and energy-dispersive X-ray (EDX) spectroscopy.

2.5. UV-Vis and FTIR Spectroscopy

The spectra of prepared CNPs were obtained using a UV-visible spectrophotometer (Thermo Fisher Scientific, India) in the wavelength range of 240–480 nm. FTIR spectroscopic analysis was carried out to determine the presence of functional groups on the surface of CNPs. FTIR characterization of CNPs was carried out in the wavelength range of 4,000–250 cm^{-1} with the help of an FTIR spectrophotometer (Perkin Elmer). The FTIR spectra were plotted as transmittance (%T) versus wavenumber (cm^{-1}).

2.6. DLS and Zeta Potential

The prepared samples were resuspended in HPLC purified water, followed by ultra-sonication for 10–15 minutes at room temperature. The particle charge and size (hydrodiameter) distribution profile of CNPs was studied using the Malvern Zetasizer Nanosystem (Worcestershire, UK).

2.7. HRTEM, EDX, and XRD analysis

HRTEM micrographs were captured using an Field Electron and Ion Company Tecnai (G2 F20) system (6×10^6 times magnification with resolutions of 0.2 Å) at 200 keV. The elemental compositions of synthesized CNPs were characterized using EDX spectroscopy in conjunction with HRTEM. The broad-angle XRD with a Cu-K-α-1 radiation source (λ = 1.540 Å) was used for the investigation over a 2θ range of 10°–80° with a scan rate of 3° per minute at 25°C.

2.8. Assay for Assessment of Antibacterial Activity

Three Gram-negative bacteria, *Escherichia coli* [Microbial Type Culture Collection (MTCC) 443], *Moraxella catarrhalis* (MTCC 445), and *Klebsiella pneumoniae* (MTCC 9544), and two Gram-positive bacteria, *Staphylococcus aureus* (MTCC 3160) and *Staphylococcus epidermidis* (MTCC 9040), were used as model organisms to assess the efficacy of antibacterial potential of CNPs. All the above mentioned bacterial cultures were procured from Institute of Microbial Technology, Chandigarh (UT), India.

2.9. Agar-Well Diffusion Assay

The agar-well diffusion assay was performed to check the efficacy of the prepared CNPs for the bactericidal activity. First of all, all the bacterial strains were grown in the MHB at 37°C for 18 hours. These strains were further reinoculated in fresh MHB (50–60 ml) at 37°C for 2–3 hours to obtain midlogarithmic phase bacteria [34,37]. These bacteria were centrifuged for 1,500–2,500 rpm at 4°C for 5–6 minutes. The pellets of bacteria were washed twice with sodium-phosphate buffer (10 mM) and resuspended in the same buffer (pH = 7.4). Concentrations of bacteria were standardized according to the formula based on the optical density measurement of the respective bacterial aliquot (OD_{620} 0.20= 5×10^7 colony-forming units/ml). Autoclaved MHA (20–25 ml) was poured into agar plates aseptically and allowed to solidify in a laminar air-flow chamber. On the agar plates, 100 µl of standardized inoculums of each test bacterium was equally spread using a sterile glass rod for confluent growth of microorganisms. Four cavities were prepared aseptically in the inoculated MHA plates. For measuring the bactericidal activity of different CNPs, 90 µl of the respective concentration of CNPs was propelled into the wells of agar containing the test bacteria and incubated for 24 hours at 37°C. The assay was performed in triplicate, and the inhibitory potential of CNPs was evaluated by determining the zone of inhibition (ZOI) around the well on a millimeter scale [mean ± standard deviation (SD)].

2.10. XTT-Colorimetric Assay

The CNPs were also evaluated for their bactericidal activity using the XTT-colorimetric method [33–35]. This method is based on the principle that the dehydrogenase enzyme of metabolically active cells has the ability to reduce XTT salt into a colored formazan, which can be measured colorimetrically at 490 nm. The change in absorbance value of this water-soluble formazan can be correlated with cell viability. In this experiment, 170 µl of the adjusted broth cultures (5×10^7 CFU/ml), as explained in the previous section, was propelled directly into a 96-well enzyme-linked immunosorbent assay (ELISA) plate. In the broth, 30 µl of CNPs solution (different concentrations) was added, mixed gently, and incubated for 14–16 hours at 37°C. After that incubation, 100 µl of each well material (after well mixing) was transferred into a new plate followed by the addition of 25 µl of a fresh XTT + menadione (12.5:1 v/v ratio) solution with gentle mixing. Finally, plates containing the reaction mixture were incubated for 2–2.5 hours at 37°C. Well readings were taken at 490 nm using an ELISA plate reader (Thermo Fisher Scientific, India). The broth with respective bacteria and without any inhibitor (antibiotic or CNPs) acts as a negative control. The experiment was performed in triplicate, and after subtracting the value of blanks, final readings were taken as mean + SD. Bactericidal effect (percentage reduction of bacterial growth) was calculated with the following formula:

% Rd = 100% – [(OD of the well- OD of the blank) ×100]./OD (negative control)

In both the abovementioned assays, antibiotic ciprofloxacin (500 µg/ml) served as the positive control. In the case of the agar-well diffusion assay, if the value of ZOI was found to be 0.5 mm or less, the effect was considered nil (no effect), whereas, in the case of the XTT-colorimetric assay, a percentage reduction value equal to or less than 5% was considered as nil (no effect).

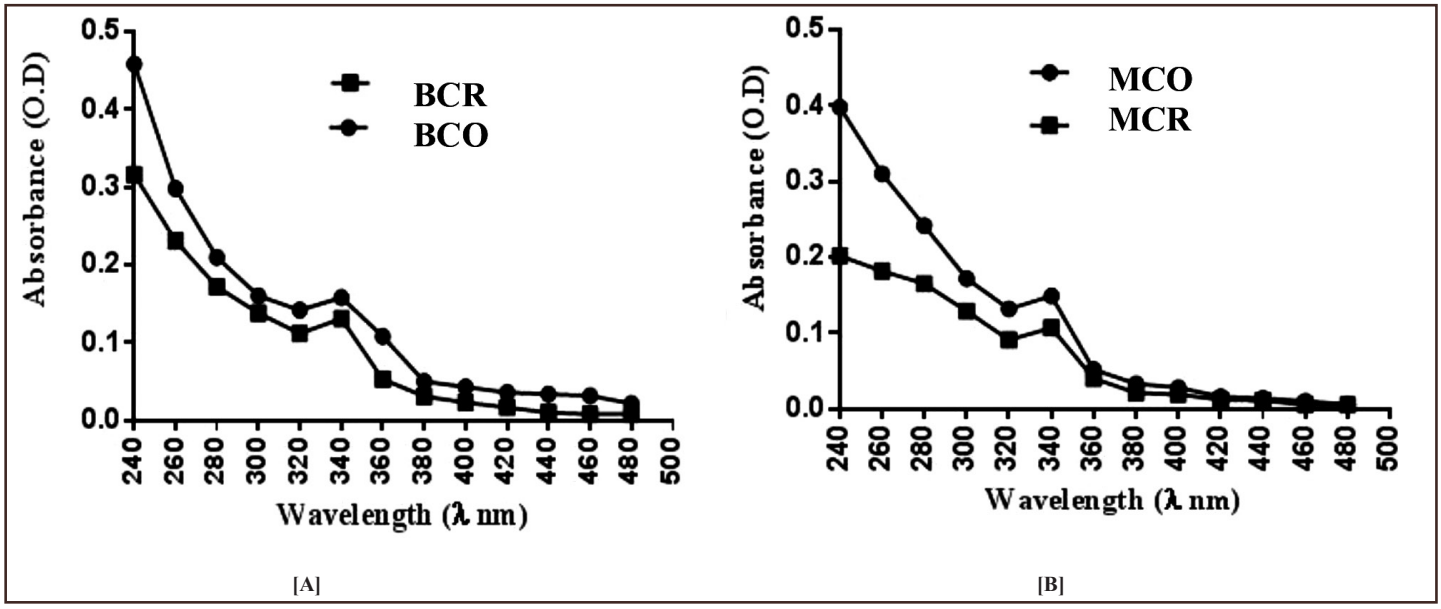

Figure 1: UV-visible spectra of CNPs. (A) Butter CNPs (raw and oxidized); (B) Mustard oil CNPs (raw and oxidized).

2.11 Assessment of Minimum Inhibitory Concentration (MIC) and minimum bactericidal concentration (MBC) Values

MIC values were evaluated for all the tested bacterial strains and determined using XTT-colorimetric readings that demonstrated the bactericidal effect of different concentrations of various CNPs [34]. The lowest concentration of CNPs, which inhibited the bacterial growth completely, was considered as the MIC. The MBC (minimum bactericidal concentration) is the lowest concentration of CNPs that was able to inhibit the growth of bacteria completely after their subculturing on antibiotic-free MHA media. In this experiment, 100 µl of contents from the selected tubes (showing complete inhibition as per XTT-colorimetric results) was cultured on MHA plates and incubated at 37°C for 24 hours to check the bacterial growth.

3. RESULTS AND DISCUSSION

3.1. UV-Vis Spectrophotometry Results

UV-vis spectrophotometry reading shows the standard CNPs-specific absorbance peaks, as shown in Figure 1. Absorbance maxima for all CNPs were found in the ranges of 240 and 340 nm. There was no noticeable change between pristine and oxidized CNPs found, except that oxidized CNPs (BCO and MCO) showed stronger absorbance at all wavelengths than pristine CNPs (BCR and MCR). However, as observed by previous studies, our CNPs exhibited a small protrusion at 340 nm (due to the n-π* transition of C = O groups present on CNPs) but did not observe any other distinct peak around 270 nm as observed by some authors [38–41].

3.2. FTIR Analysis

The FTIR spectrum identifies chemical bonds or functional groups attached to a molecule and hence acts as a distinctive molecular fingerprint of that particular molecule. The FTIR transmittance spectra of pristine and nitric acid oxidized CNPs showed three significant regions of peaks: 1,300–800 cm^{-1} attributed to various C–O single bonds, 2,000–1,300 cm^{-1} ascribed to different oxygen functional groups, and 4,000–2,000 cm^{-1} due to various dehydration and aliphatic units (Fig. 2). A broad and intense peak at 3,401–3,420 cm^{-1} corresponds to symmetric vibrations of the O–H group in a cyclic structure [38,40]. Peaks at 3,391–3,396 cm^{-1} were present due to the stretching vibrations of N–H groups [36]. Peaks at 2,911–2,926 cm^{-1} were ascribed to stretching vibration of the C–H groups of aliphatic carbon [40–42]. Peaks observed in the region of 2,508–2,544 cm^{-1} were due to overtones and combinations of in-plane bending of the O–H group and stretching vibrations of the C–O group [38]. Peaks in the range of 3,748–3,854 cm^{-1} comprise –O–H (due to adsorbed moisture) group stretching [43].

The broadband observed in 1,723–1,729 cm^{-1} was assigned to stretching vibration of C = O (carbonyl) groups, and peaks at 1,615–1,662 cm^{-1} were present due to the presence of asymmetric stretching vibration of the C–OH (carboxyl) group of carboxylic acid [1,38]. Peaks in the region of 1,234–1,241 cm^{-1} were attributed to the presence of C–N stretching/bending and peaks observed around 1,009–1,015 cm^{-1} were ascribed to the presence of = C–H skeletal vibration [38]. Our study did not observe peaks at 2,340 and 2,343 cm^{-1} which were ascribed to carbon dioxide from unburnt hydrocarbons present in soot [36]. Peaks in the region of 677–683 cm^{-1} relate to the alkyl halides band, especially the C–Cl bond. Overall, peaks at 3,391–3,420 cm^{-1} (O–H stretching), 1,615–1,662 cm^{-1} (carboxyl group), and 1,723–1,729 cm^{-1} (carbonyl group) along with the peak at 1,384 cm^{-1} (attributed to stretching of the C–N bond present in aromatic amine groups) indicate that the synthesized CNPs were capped and stabilized by these groups [38,40,41], which further prevents their agglomeration and hence their stabilization in various solvents.

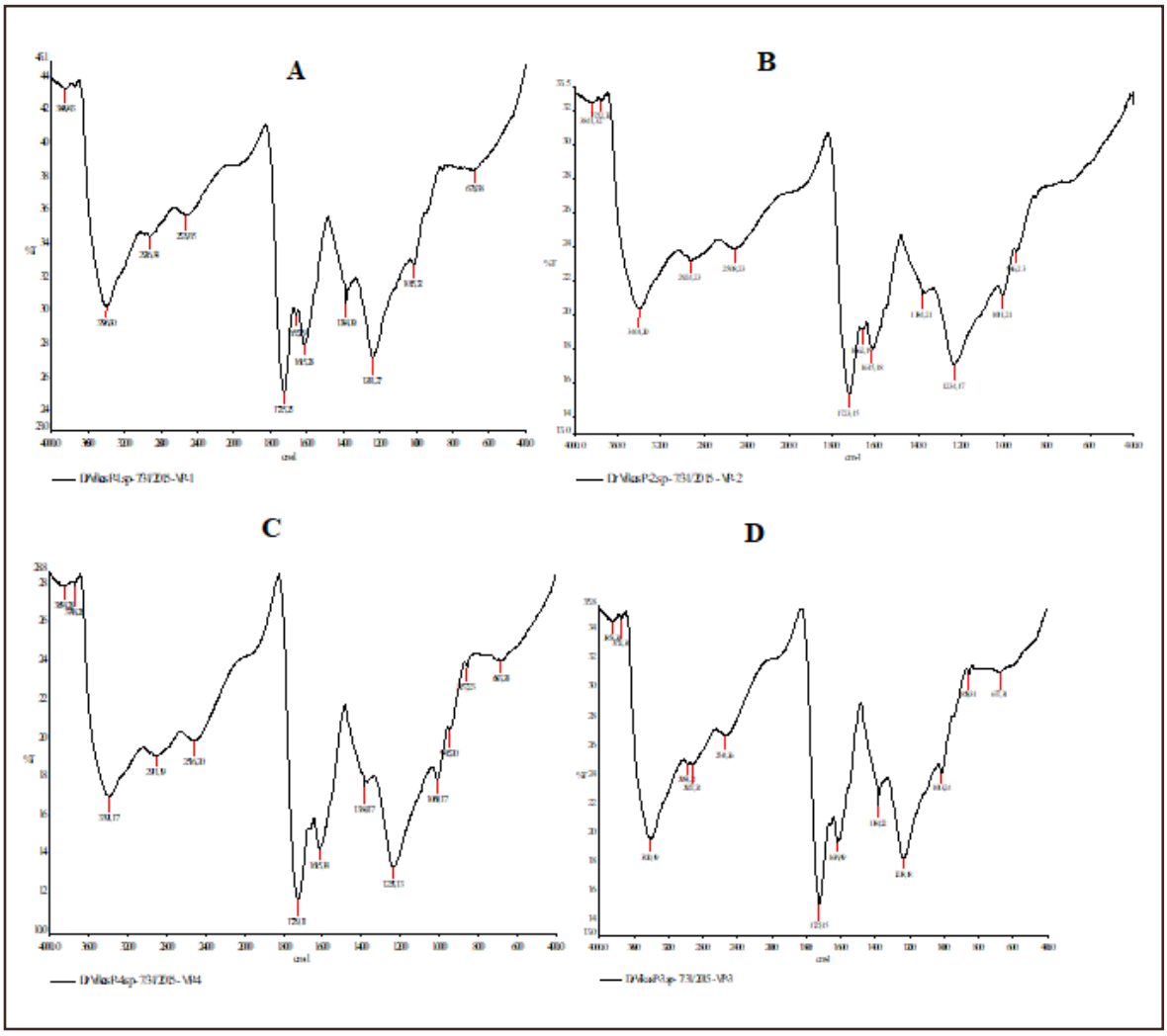

Figure 2: FTIR spectra of various CNPs. (A) BCR; (B) BCO; (C) MCR; (D) MCO.

3.3. DLS and Zeta Potential

DLS was used to estimate the size (average hydrodiameter) distribution profile of small CNPs in the dispersion medium. CNPs from butter, i.e., BCP and BCO, were found in the ranges of 62.65 and 36.43 nm, respectively (Fig. 3), whereas MCP and MCO were observed to have average diameters of 108.4 and 69.17 nm, respectively, as shown in Figure 4. A high value of zeta potential confers stability of solution containing CNPs, which means solution resists aggregation of CNPs, whereas small zeta potential values indicate the formation of coagulation/flocculation in the solution. In our study, zeta potentials of BCR and BCO were found to be −9.05 and −14.6 mV, respectively (Fig. 3), whereas MCR and MCO were found to possess zeta potential values −12.7 and −20.1 mV, respectively (Fig. 4). The higher value of zeta potential of nitric acid oxidized CNPs is responsible for their higher stability, good colloidal stability, and more hydrophobic nature than pristine CNPs. Furthermore, nitric acid oxidation helps in the splitting of large aggregated CNPs into smaller ones [36]. Previously, synthesized CNPs (CDs and carbon nanospheres) were shown to have zeta potential in the ranges of −11.9 [43], −10.4 [6], and −10.34 mV [39].

3.4. HRTEM/EDX

HRTEM analysis describes the information regarding the size and shape of CNPs. The size and morphology of synthesized CNPs were determined by HRTEM at both low and high resolutions, and the resulting monographs are shown in Figures 5 and 6. Sizes of the synthesized BCR and BCO CNPs were observed in the ranges of 10–90 and 5–20 nm, respectively (Fig. 5), whereas the sizes of MCR and MCO CNPs were found in the ranges of 100–150 and 50–70 nm, respectively as shown in Figure 6. HRTEM images (Fig. 5) demonstrated that there seems to be an aggregation or agglutination of small CNPs (5–10 nm makes a bunch of 50–60 nm sized CNPs) in the case of raw CNPs from butter (BCR). In the case of MCR (Fig. 6), it was observed that CNPs were interconnected and were spherical in shape. Some CNPs were like suppressed carbon balls on both sides. HRTEM analysis also demonstrated a fractal-like short-branched nanochain (Fig. 6C). As per literature, strong diffusive forces are responsible for forming and stabilizing such structures [1,44]. HRTEM results corroborate the DLS observations regarding the size distribution profile of synthesized CNPs as described in Section 2. DLS

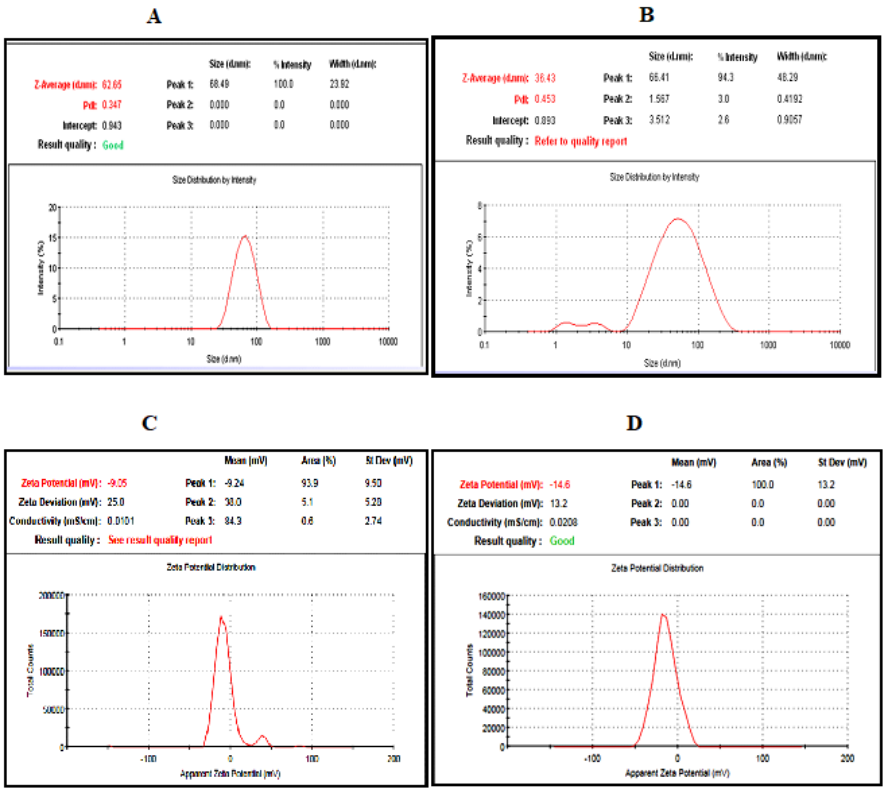

Figure 3: DLS and zeta potential spectra of butter CNPs. (A) DLS of BCR; (B) DLS of BCO; (C) Zeta potential of BCR; (D) Zeta potential of BCO.

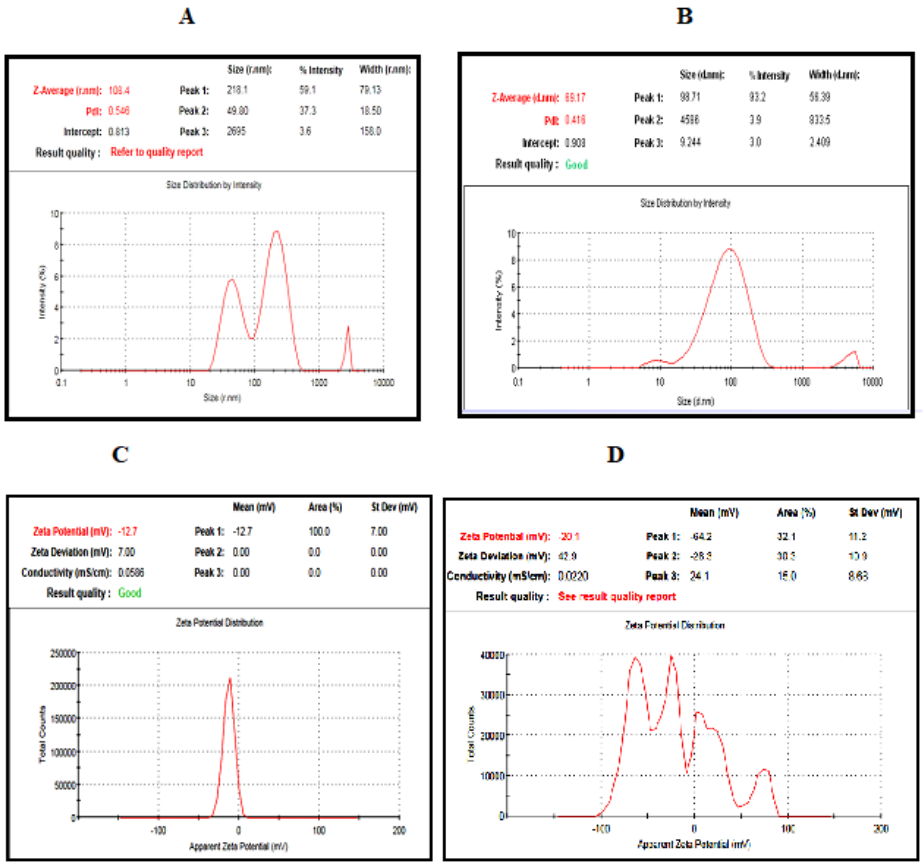

Figure 4: DLS and zeta potential spectra of mustard oil CNPs. (A) DLS of MCR; (B) DLS of MCO; (C) Zeta potential of MCR; (D) Zeta potential of MCO.

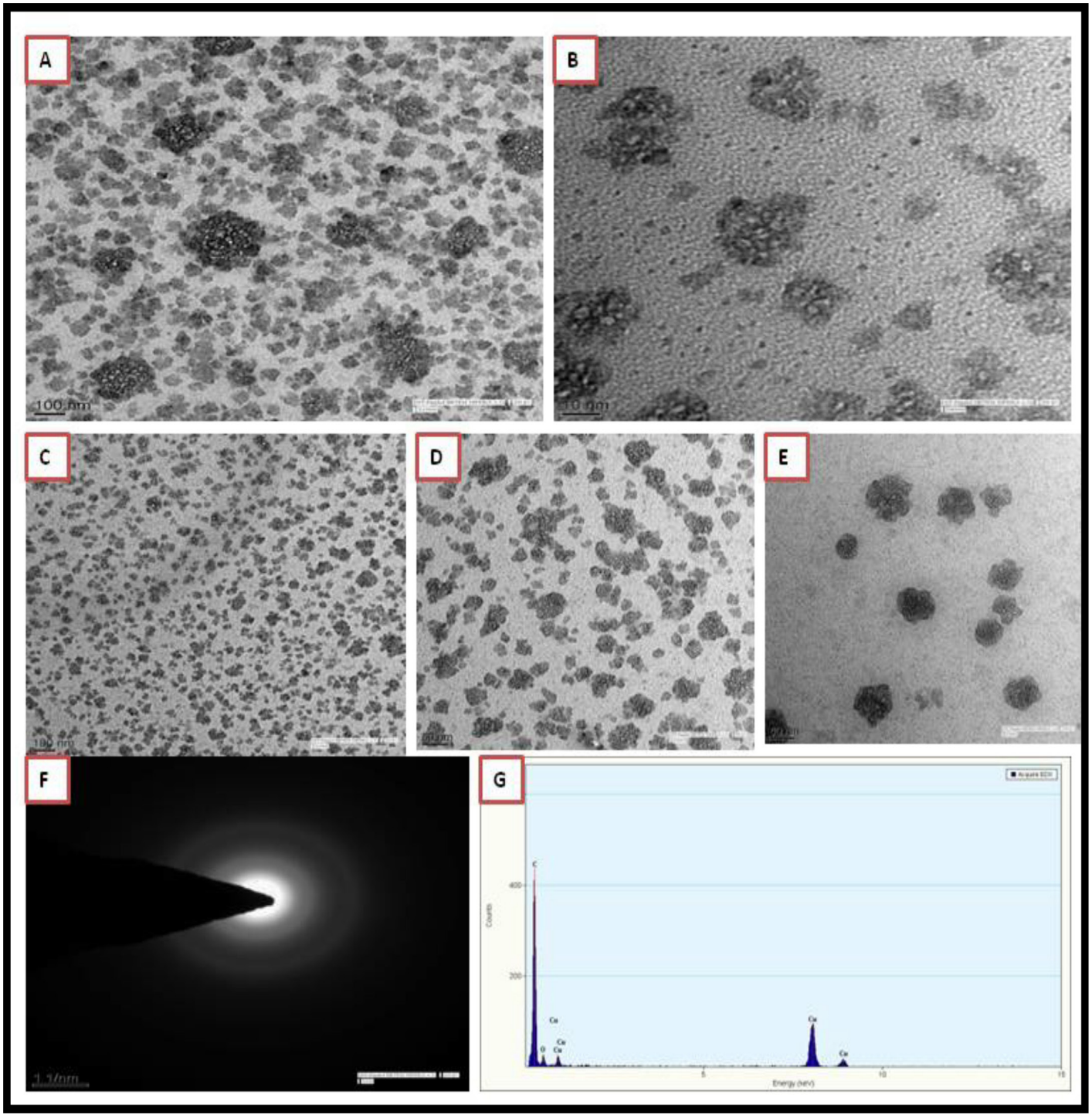

Figure 5: HRTEM micrograph of butter CNPs (A) HRTEM micrograph of BCR at 100 nm and (B) at 10 nm; (C) HRTEM micrograph of BCO at 100 nm; (D) at 50 nm and (E) at 20 nm. SAED pattern (F) and EDX micrograph (G).

estimates the overall hydrodynamic diameter of NPs along with adsorbed ions and molecules present on their surface; hence, the estimated size of NPs was found to be larger than that predicted by HRTEM results. The EDX spectrum described the elemental analysis of synthesized CNPs (Figs. 5G and 6H) and showed the presence of only carbon and oxygen, and no impurities of other elements like sulfur, chlorine, calcium, magnesium, sodium, and potassium were found as observed by some authors who synthesized CNPs from the kitchen or oil soot [45,46].

3.5. XRD

The XRD spectrum revealed structural characterization and lattice phase information of synthesized CNPs (Fig. 7). In all CNPs from the present study, we observed two prominent

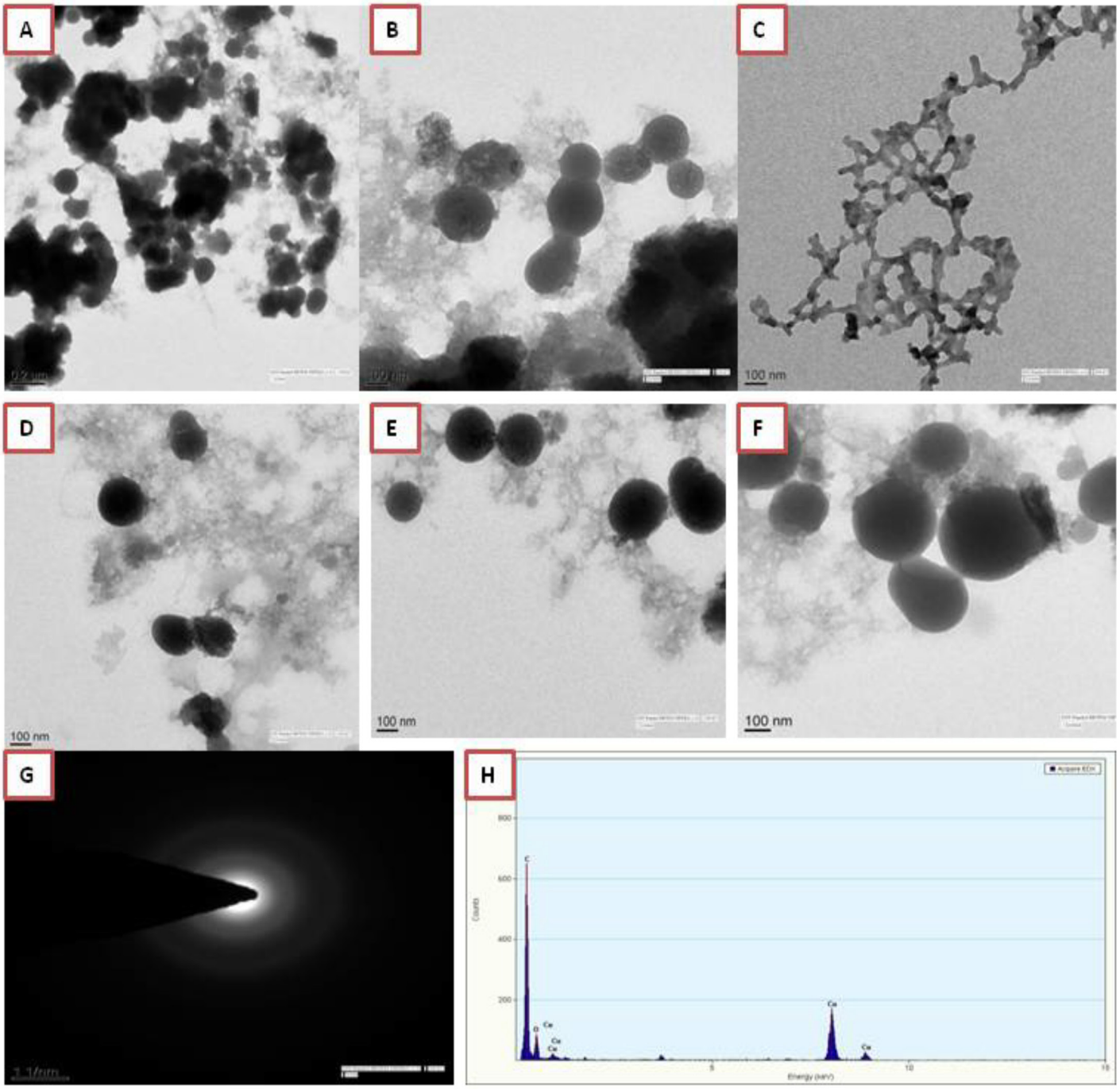

Figure 6: HRTEM micrograph of mustard oil CNPs (A) HRTEM micrograph of MCR at 0.2 um and (B) at 100 nm; (C) fractal-like nanochain. HRTEM micrograph of MCO at 100 nm (D), (E), and (F). SAED pattern (G) and EDX micrograph (H).

diffraction peaks: a high-intensity peak centered around 25° which is ascribed to the (002) indices and a second low-intensity peak around 43° which corresponds to the (100) indices. The broad peak at 25° revealed that the CNPs are of predominantly amorphous material with a graphene layer, whereas the prominent low peak at 43° confirmed the graphitic crystalline nature of CNPs [25,39]. The selected area electron diffraction (SAED) pattern in concordance with the XRD results showed the presence of a dot-like crystalline structure, which confirmed the graphitic crystalline nature of synthesized CNPs (Figs. 5F and 6G). It has been suggested that these kinds of CNPs, i.e., hybridized graphitic CNPs, have tremendous applications in various fields like sensing, imaging, and photothermal therapeutics [1,43].

3.6. Antibacterial Activity of CNPs

Raw and oxidized CNPs from butter (BCR and BCO) exhibited their bactericidal effect against all the five tested bacterial strains (Table 1, Figs. 8 and 9). At the highest concentration (3

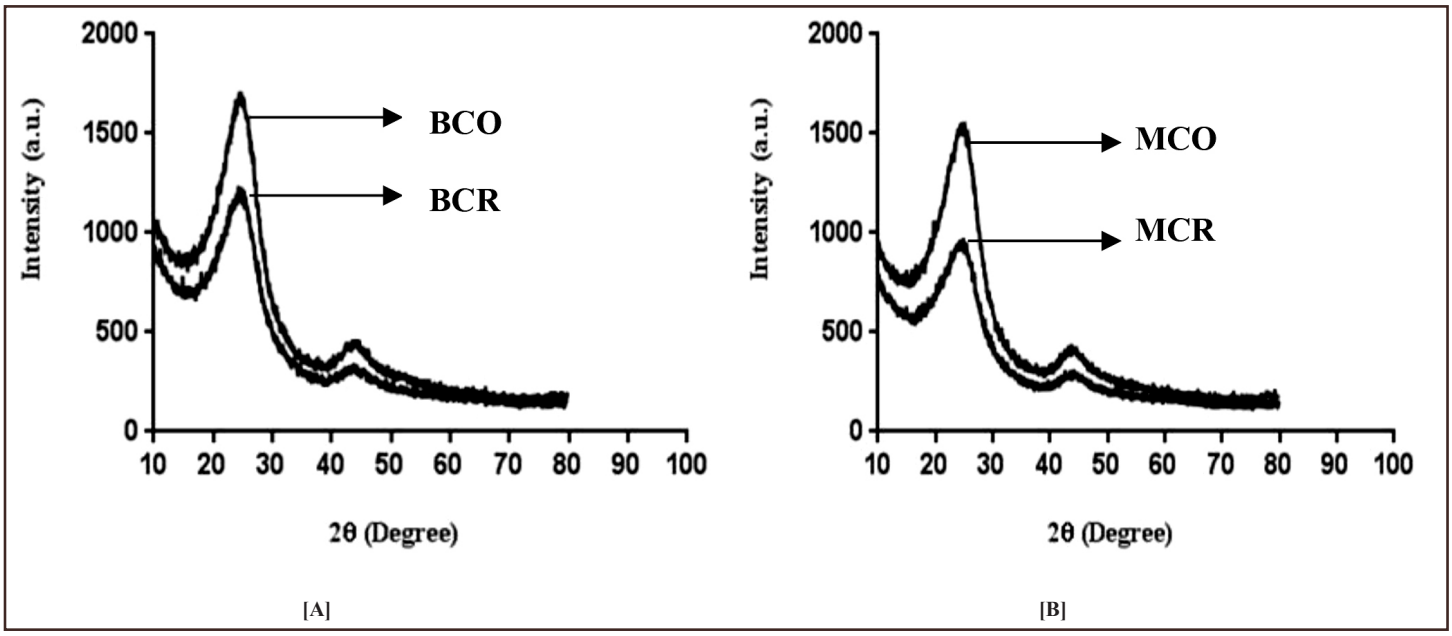

Figure 7: XRD results of (A) BCR and BCO; (B) MCR and MCO.

Table 1: Comparative analysis of ZOI produced by different types of carbon NPs against pathogenic bacteria in agar-well diffusion assay.

Bacteria	ZOI (mm ± SD)				
	CNPs	3 mg/ml	2 mg/ml	1 mg/ml	0.50 mg/ml
Escherichia coli	MCR	6.5 ± 0.5	3.5 ± 0.5	1.5 ± 0.5	No effect (NE)
	MCO	9.66 ± 0.57	7.16 ± 0.28	5.83 ± 0.28	3.33 ± 0.28
	BCR	7.33 ± 0.57	6.16 ± 0.28	4.16 ± 0.28	2.0 ± 0.0
	BCO	10.83 ± 0.28	9.5 ± 0.5	7.5 ± 0.5	3.16 ± 0.28
Staphylococcus aureus	MCR	6.5 ± 0.5	4.66 ± 0.57	2.83 ± 0.28	1.00 ± 0.0
	MCO	9.16 ± 0.28	7.16 ± 0.28	6.5 ± 0.5	3.0 ± 0.0
	BCR	8.66 ± 0.57	5.16 ± 0.28	4.83 ± 0.28	2.0 ± 0.0
	BCO	13.5 ± 0.5	11.16 ± 0.28	8.66 ± 0.57	4.0 ± 0.0
Klebsiella pneumoniae	MCR	5.66 ± 0.57	3.83 ± 0.28	1.83 ± 0.28	1.16 ± 0.28
	MCO	7.83 ± 0.28	5.5 ± 0.5	3.83 ± 0.28	3.0 ± 0.0
	BCR	6.5 ± 0.5	4.83 ± 0.28	2.16 ± 0.28	1.00 ± 0.0
	BCO	9.5 ± 0.5	7.5 ± 0.5	6.16 ± 0.28	3.66 ± 0.57
Moraxella catarrhalis	MCR	5.16 ± 0.28	3.16 ± 0.28	2.0 ± 0.0	NE
	MCO	8.5 ± 0.5	6.16 ± 0.28	4.83 ± 0.28	2.16 ± 0.28
	BCR	6.16 ± 0.28	4.83 ± 0.28	3.16 ± 0.28	1.16 ± 0.28
	BCO	10.83 ± 0.28	8.66 ± 0.57	5.16 ± 0.28	2.5 ± 0.5
Staphylococcus epidermidis	MCR	4.16 ± 0.28	2.83 ± 0.28	1.5 ± 0.5	1.00 ± 0.0
	MCO	6.16 ± 0.28	4.5 ± 0.5	3.5 ± 0.5	1.5 ± 0.0
	BCR	5.16 ± 0.28	4.16 ± 0.28	2.83 ± 0.28	1.00 ± 0.0
	BCO	6.83 ± 0.28	3.83 ± 0.28	3.16 ± 0.28	2.5 ± 0.5

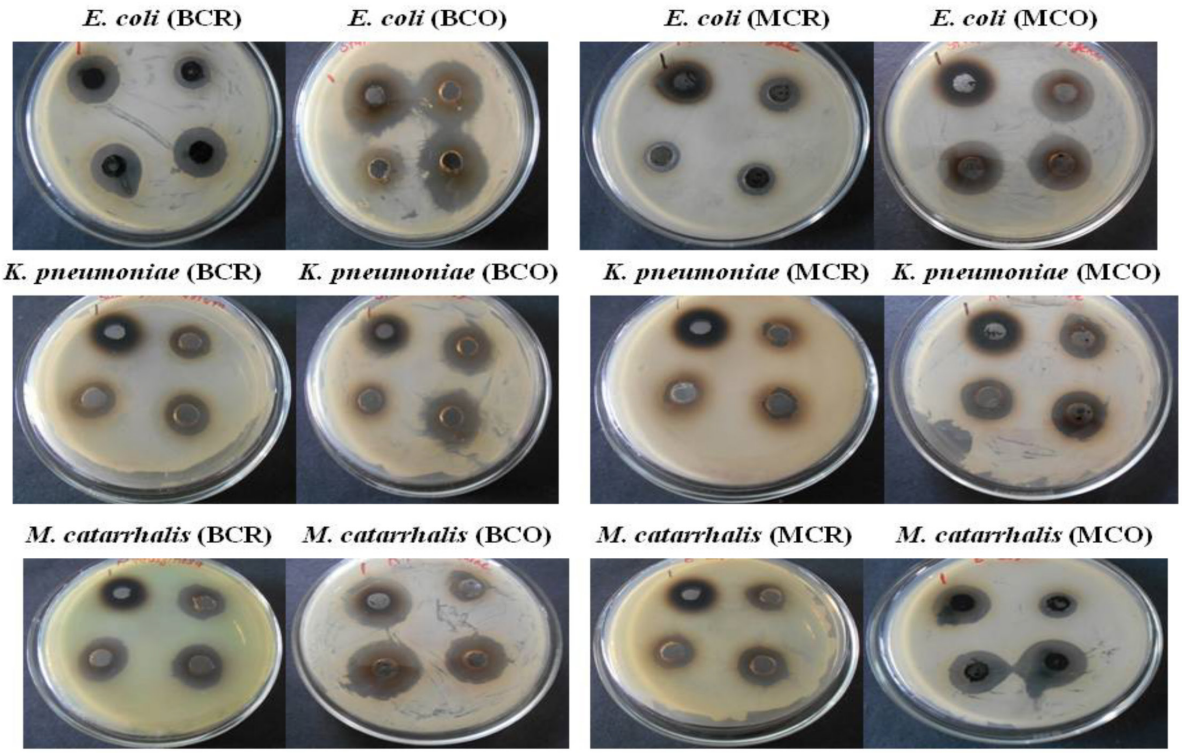

Figure 8: Agar-well diffusion results showing the bactericidal effect of different kinds of CNPs against Gram-negative bacteria.

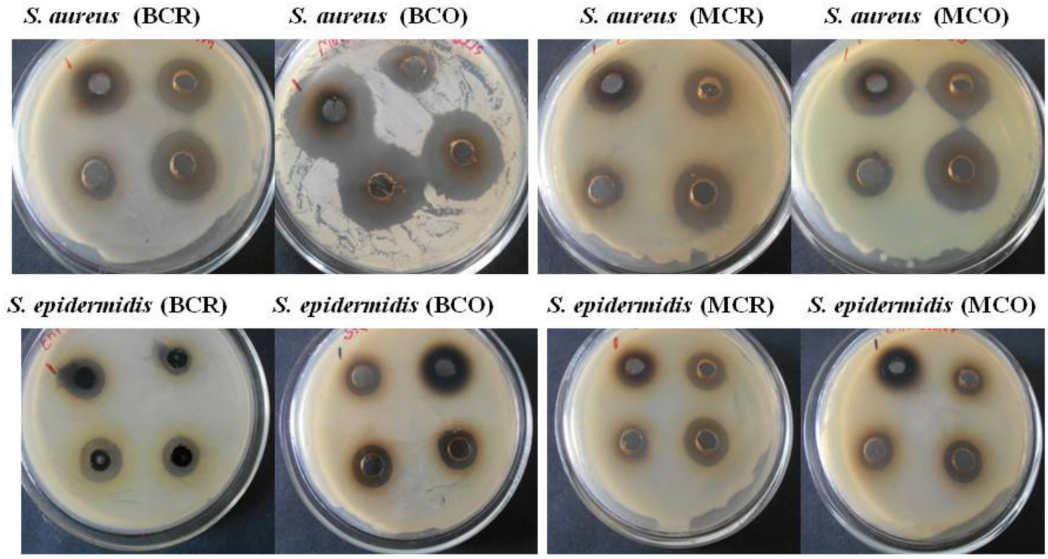

Figure 9: Agar-well diffusion results showing the bactericidal effect of different kinds of CNPs against Gram-positive bacteria.

mg/ml), BCR exhibited bactericidal efficiency in the order of *S. aureus* (8.66 + 0.57 mm) followed by *E. coli* (7.33 + 0.57 mm) > *K. pneumoniae* (6.5 + 0.5 mm) > *M. catarrhalis* (6.16 + 0.28 mm) > *S. epidermidis* (5.16 + 0.28 mm). In the case of BCO, at the highest concentration (3 mg/ml), CNPs (CDs) demonstrated their profound bactericidal potential in the order of *S. aureus* (13.5 + 0.5 mm) > *E. coli* and *M. catarrhalis* (10.83 + 0.28 mm) > *K. pneumoniae* (9.5 + 0.5 mm) and were least effective against *S. epidermidis* (6.83 + 0.28 mm). XTT-colorimetric results (Tables 2 and 3) demonstrated that, at the highest concentration (800 µg/ml), BCO completely killed the bacteria *K. pneumoniae*, *M. catarrhalis*, and *S. aureus*, whereas in the case of *E. coli* and *S. epidermidis* the percentage reduction was observed in the ranges of 97.45% and 84.16%, respectively. Up to the concentration of 25 µg/ml, BCO exerted a low level of bactericidal effect against *S. aureus* (Rd: 24.44%), *M. catarrhalis* (Rd: 16.64%), and *K.*

Table 2: Measurement of O.D of growth (mean ± SD) of different gram (+/-) bacteria at various concentrations of different CNPs.

Bacteria	PC	NC	NPs	800 µg/ml	400 µg/ml	200 µg/ml	100 µg/ml	50 µg/ml	25 µg/ml
Staphylococcus aureus	0.064 ± 0.016	0.796 ± 0.035	BCO	0.003 ± 0.002	0.034 ± 0.011	0.141 ± 0.014	0.336 ± 0.039	0.454 ± 0.020	0.601 ± 0.027
			BCR	0.069 ± 0.013	0.182 ± 0.012	0.459 ± 0.009	0.676 ± 0.014	NE	NE
	0.079 ± 0.010	0.826 ± 0.045	MCO	0.008 ± 0.002	0.145 ± 0.010	0.302 ± 0.013	0.519 ± 0.018	0.686 ± 0.013	NE
			MCR	0.169 ± 0.011	0.282 ± 0.029	0.510 ± 0.032	0.662 ± 0.044	NE	NE
Moraxella catarrhalis	0.105 ± 0.015	0.858 ± 0.012	BCO	0.006 ± 0.003	0.077 ± 0.014	0.206 ± 0.013	0.322 ± 0.016	0.530 ± 0.031	0.715 ± 0.020
			BCR	0.061 ± 0.017	0.292 ± 0.032	0.530 ± 0.013	0.756 ± 0.0263	NE	NE
	0.067 ± 0.011	0.908 ± 0.030	MCO	0.065 ± 0.014	0.239 ± 0.036	0.462 ± 0.031	0.727 ± 0.024	NE	NE
			MCR	0.228 ± 0.017	0.539 ± 0.023	0.662 ± 0.036	0.845 ± 0.018	NE	NE
Escherichia coli	0.082 ± 0.014	0.903 ± 0.016	BCO	0.023 ± 0.007	0.165 ± 0.012	0.385 ± 0.018	0.621 ± 0.010	0.822 ± 0.018	NE
			BCR	0.224 ± 0.020	0.565 ± 0.013	0.794 ± 0.034	NE	NE	NE
	0.097 ± 0.005	0.796 ± 0.031	MCO	0.098 ± 0.009	0.303 ± 0.017	0.618 ± 0.030	0.723 ± 0.028	NE	NE
			MCR	0.273 ± 0.042	0.488 ± 0.021	0.671 ± 0.036	NE	NE	NE
Klebsiella pneumoniae	0.061 ± 0.015	0.879 ± 0.014	BCO	0.007 ± 0.002	0.095 ± 0.010	0.292 ± 0.035	0.468 ± 0.026	0.590 ± 0.046	0.754 ± 0.024
			BCR	0.115 ± 0.015	0.326 ± 0.013	0.539 ± 0.016	0.759 ± 0.025	NE	NE
	0.108 ± 0.012	0.856 ± 0.026	MCO	0.089 ± 0.010	0.289 ± 0.022	0.407 ± 0.039	0.519 ± 0.041	0.745 ± 0.024	NE
			MCR	0.302 ± 0.011	0.490 ± 0.017	0.595 ± 0.014	0.713 ± 0.023	NE	NE
Staphylococcus epidermidis	0.077 ± 0.036	0.891 ± 0.061	BCO	0.141 ± 0.023	0.276 ± 0.031	0.526 ± 0.019	0.725 ± 0.047	NE	NE
			BCR	0.260 ± 0.049	0.516 ± 0.028	0.778 ± 0.018	NE	NE	NE
	0.090 ± 0.009	0.826 ± 0.029	MCO	0.248 ± 0.014	0.499 ± 0.033	0.637 ± 0.027	0.761 ± 0.043	NE	NE
			MCR	0.353 ± 0.020	0.530 ± 0.056	0.695 ± 0.031	NE	NE	NE

pneumoniae (Rd: 14.20%) and no effect against *E. coli* and *S. epidermidis*. BCR at the concentration of 800 µg/ml was found to be an effective bactericidal agent in the order of *M. catarrhalis* (Rd: 92.89%) > *S. aureus* (Rd: 91.33%) > *K. pneumoniae* (Rd: 86.91%) > *E. coli* (Rd: 75.16%) > *S. epidermidis* (Rd: 70.72%). In comparison to BCO, BCR exhibited a passable bactericidal effect against the tested strains at a concentration of 100 µg/ml in the order of *S. aureus* (Rd: 15.05%) > *K. pneumoniae* (Rd: 13.64%) > *M. catarrhalis* (Rd: 11.86%) and no effect against *E. coli* and *S. epidermidis*. As per the agar-well diffusion and XTT-colorimetric results, the bactericidal effect of BCO was more profound than that of BCR.

The agar-well diffusion results of CNPs from mustard oil (MCR and MCO) showed that (Figs. 8 and 9 and Table 1), at the highest concentration (3 mg/ml), MCR was observed to be equally effective against *E. coli* and *S. aureus* (6.5 + 0.5 mm), followed by *K. pneumoniae* (5.66 + 0.57 mm), *M. catarrhalis* (5.16 + 0.28 mm), and *S. epidermidis* (4.16 + 0.28 mm). In the case of MCO, at the highest concentration (3 mg/ml), CNPs (carbon nanospheres) were observed to be effective in the order of *E. coli* (9.66 + 0.57 mm) followed by *S. aureus* (9.16 + 0.28 mm) > *M. catarrhalis* (8.5 + 0.5 mm) > *K. pneumoniae* (7.83 + 0.28 mm) > *S. epidermidis* (6.16 + 0.28 mm). In case of mustard CNPs (Table 3), as per XTT results, at the 800 µg/ml concentration, MCO exhibited complete inhibition against *S. aureus* followed by *M. catarrhalis* (Rd: 92.74%) > *K. pneumoniae* (Rd: 89.60%) > *E. coli* (Rd: 87.61%) > *S. epidermidis* (Rd: 69.95%). MCO at the concentration of 50 µg/ml showed a passable bactericidal

Table 3: Percentage reduction (%) of different bacterial strains in the presence of various concentrations of different types of CNPs.

Bacteria	PC	CNPs	800 µg/ml	400 µg/ml	200 µg/ml	100 µg/ml	50 µg/ml	25 µg/ml
Staphylococcus aureus	91.95	BCO	Complete inhibition (CM)	95.72	82.28	57.78	42.96	24.44
		BCR	91.33	77.13	42.25	15.05	NE	NE
	90.43	MCO	CM	82.37	63.37	37.12	16.92	NE
		MCR	79.43	65.78	38.24	19.83	NE	NE
Moraxella catarrhalis	87.76	BCO	CM	91.02	75.99	62.47	38.22	16.64
		BCR	92.89	65.94	38.18	11.86	NE	NE
	92.62	MCO	92.74	73.61	49.05	19.84	NE	NE
		MCR	74.88	40.56	27.04	6.92	NE	NE
Escherichia coli	90.91	BCO	97.45	81.69	57.31	31.22	8.92	NE
		BCR	75.16	37.33	11.97	NE	NE	NE
	87.81	MCO	87.61	61.83	22.26	9.12	NE	NE
		MCR	65.65	38.65	15.63	NE	NE	NE
Klebsiella pneumoniae	93.06	BCO	CM	89.19	66.78	46.75	32.77	14.20
		BCR	86.91	62.87	38.67	13.64	NE	NE
	87.38	MCO	89.60	66.16	52.38	39.29	12.90	NE
		MCR	64.69	42.75	30.45	16.63	NE	NE
Staphylococcus epidermidis	91.35	BCO	84.16	69.02	40.89	18.54	NE	NE
		BCR	70.72	42.07	12.66	NE	NE	NE
	89.10	MCO	69.95	39.49	22.84	7.76	NE	NE
		MCR	57.18	35.81	15.78	NE	NE	NE

effect against *S. aureus* (16.92%) and *K. pneumoniae* (12.90%), whereas bacteria *M. catarrhalis*, *E. coli*, and *S. epidermidis* remain unaffected. MCR at the concentration of 800 µg/ml demonstrated an inhibitory effect in the order of *S. aureus* (Rd: 79.43%) > *M. catarrhalis* (Rd: 74.88%) > *E. coli* (Rd: 65.65%) > *K. pneumoniae* (Rd: 64.69%) > *S. epidermidis* (Rd: 57.18%). MCR was found effective (low-level) only up to the concentration of 100 µg/ml against *S. aureus* (Rd: 19.83%), *K. pneumoniae* (Rd: 16.63%), and *M. catarrhalis* (Rd: 6.92%). In this case also, oxidized CNPs, i.e., MCO, were found to have more profound bactericidal potency than raw CNPs (MCR), as depicted in Table 1.

It has been postulated and successfully demonstrated in several studies that carbon nanostructures-mediated bactericidal mechanism may involve any one or combination of the following mechanisms: a) the hydrophobic surface of carbon nanostructures interacts with bacterial membrane lipids and intercalates them which results in irreparable pore formations and death of bacteria; b) after internalization of the CNPs into the bacteria they may impair the respiratory chain by inhibiting various enzymes by direct oxidation or by involving reactive oxygen species- (ROS-) mediated oxidation of cellular components which results in the loss of cellular structural integrity and death of bacteria [41,47]; c) the third mechanism believed that these nanostructures directly pierce cell membrane and disrupt the bacterial cell wall which is responsible for their bactericidal effect [48,49]. Liu *et al.* [50] demonstrated through atomic force microscopy images that CNTs-mediated bacterial death involves the bacterial cell membrane's piercing. Moreover, CNPs-mediated killing of bacterial cells depends on the size, shape, concentration of CNPs, reaction media, and bacterial strains. What we observed from the results of various studies is that CDs (< 10 nm) which have the ability to cross the bacterial cell membrane may exert their bactericidal effect through ROS-mediated oxidative stress, and carbon nanospheres or particles with a larger size than that of bacterial cell membrane pores may kill the bacterial strains through interaction with bacterial membrane and making irreparable pores by intercalating the membrane lipids. In the case of CNTs-mediated bactericidal effect, the process may involve direct piercing of the bacterial membrane. In the present study, CNPs (CDs) exerted a more profound bactericidal effect than that of large CNPs (carbon nanospheres >50 nm), and this result could be correlated with their small size (< 10 nm).

Many groups studied the antibacterial effect of CNPs and nanostructures [single-walled and multiple-walled CNTs

(SWCNTs and MWCNTs)]. Varghese *et al.* [51] demonstrated that CNPs synthesized from kitchen soot have a strong bactericidal effect against four bacteria: *Pseudomonas aeruginosa* (22.0 mm), *Proteus refrigere* (29.0 mm), *S. aureus* (20.0 mm), and *Staphylococcus haemolyticus* (20.0 mm). Similarly, CNPs synthesized from chimney soot were found to have a promising bactericidal effect against bacteria like *S. aureus* (21.0 mm), *Streptococcus pyogenes* (15.0 mm), *K. pneumoniae* (21.0 mm), and *Proteus mirabilis* (22.0 mm) and *E. coli* (12.0 mm) up to the concentration of 250 µg/ml [52]. Mohanty *et al.* [45] showed that CNPs reduced the growth of *K. pneumoniae* up to 79.45% but have little effect on *S. aureus*. Similar to these results, henna-derived CDs produced ZOI of 15.0 and 21.0 nm against *S. aureus* and *E. coli*, respectively, at the concentration of 1 mg/ml [42]. Recently, Gao *et al.* [41] established that CDs at the concentration of 700 µg/ml completely killed the *S. aureus* bacteria. In our results, at the concentration of 800 µg/ml, BCO-mediated toxicity completely killed *S. aureus*, *K. pneumoniae*, and *M. catarrhalis* as discussed in Results. Similarly, at the same concentration (800 µg/ml), MCO completely inhibited the growth of *S. aureus*. Overall, BCO-mediated inhibition was found more profound in comparison to MCO-mediated inhibition in our results.

Su *et al.* [53] demonstrated that the bactericidal effect of CDs was size specific, where CDs with size <15 nm were found to penetrate the plasma membrane and to cause oxidative stress more efficiently than 50 nm sized carbon nanospheres [54]. In the case of the sensitivity of CNPs towards Gram-positive or Gram-negative bacteria, Jiang *et al.* [55] demonstrated that Gram-negative bacteria like *E. coli* and *P. aeruginosa* were found more resistant (MIC >200 µg/ml) than Gram-positive bacteria *S. aureus* and *Micrococcus luteus* (MIC: 2–5 µg/ml). Similarly, Shah *et al.* [42] demonstrated that whereas *E. coli* (Gram-negative) showed inhibition (ZOI) only at the 1 mg/ml concentration, Gram-positive bacteria *S. aureus* started showing ZOI from a concentration as low as 200 µg/ml. However, contrary to these studies, Dong *et al.* [9] did not observe such difference based on the Gram-positive or Gram-negative attribute of bacteria. Rather, they observed the same MIC value, i.e., 64 *µg/ml,* in the case of both Gram-negative (*E. coli*) and Gram-positive (*Bacillus subtilis*) bacteria. In the present research, we also did not observe such a difference. Herein, *S. aureus* and *S. epidermidis* (both Gram-positive) were found the most sensitive and most resistant bacteria, respectively, towards CNPs-mediated killing.

In the case of BCO, both MIC and MBC values were found to be 800 µg/ml against bacteria *K. pneumoniae*, *M. catarrhalis*, and *S. aureus* and 1 mg/ml in the case of *E. coli* and *S. epidermidis*. In the case of BCR, MIC and MBC values were observed in the concentration ranges of 1,000 and 1.5 mg/ml, respectively, against *M. catarrhalis*, *S. aureus*, and *K. pneumoniae*. *Escherichia coli* and *S. epidermidis* were the most resistant bacteria with both MIC and MBC values (BCR) in the range of 1.5 mg/ml. MCO exhibited both MIC and MBC values in the range of 800 µg/ml against *S. aureus* and 2 mg/ml against *S. epidermidis*. In the case of *M. catarrhalis*, *K. pneumoniae*, and *E. coli*, MIC and MBC values were recorded in the ranges of 1,000 and 1.5 mg/ml, respectively. Similarly, in the case of MCR, both MIC and MBC values were assessed to be 1.5 mg/ml against *S. aureus* and *M. catarrhalis* and 2 mg/ml against *E. coli*, *K. pneumoniae*, and *S. epidermidis*. Overall, MIC and MBC values were found in the order of MCR > BCR > MCO > BCO in the present study.

SWCNTs and MWCNTs are the most studied carbon nanostructures with respect to their antimicrobial property. Various studies explicated the bactericidal potential of functionalized (cationic and anionic group) and nonfunctionalized CNTs. For example, it was elucidated that covalent (lysine and arginine) functionalized MWCNTs have 1.1–2.64 times more profound antifungal effect than pristine MWCNTs against ten fungal strains like *Aspergillus niger*, *Aspergillus fumigatus*, *Penicillium chrysogenum*, *Candida albicans*, *Fusarium culmorum*, *Saccharomyces cerevisiae*, *Trichophyton mentagrophytes*, *Microsporum canis*, *Purpureocillium lilacinum*, and *Trichophyton rubrum* [56]. The reason for this remarkable increase in fungicidal efficiency is that more positively charged SWCNTs and MWCNTs could improve the adsorption of nanotubes to negatively charged bacterial membrane, which further increases their killing effect [56–58]. Furthermore, Arias and Yang [59] observed that SWCNTs with –OH and –COOH surface groups have improved bactericidal effects against certain pathogenic bacterial strains. As both –OH and –COOH groups were present on all types of CNPs from the present study, this could be one of the reasons behind their improved bactericidal effect against diverse kinds of bacterial strains.

As per CDC reports [60], in the USA alone, multidrug-resistant bacteria caused 2.8 million new infections and 35,000 deaths [21]. The World Health Organization Global Surveillance Report (2014) on Antibiotic Resistance estimates that in Southeast Asia nearly 81% of the population has developed multidrug resistance towards various bacteria such as *S. aureus*, *E. coli*, and *K. pneumoniae* [24]. This situation would create a substantial economic burden on every nation and have drastic effects on the biomedical and healthcare sector. *Klebsiella pneumoniae*, *S. aureus*, *S. epidermidis*, and *E. coli* mainly caused urinary, respiratory tract, and skin infections [21,61]. Besides these preferable sites of infections, *K. pneumoniae*, *S. aureus*, *S. epidermidis*, and *M. catarrhalis* were found to cause ocular infection in neonates, children, and adults. Traditionally, in Southeast Asia, mainly in India, Pakistan, and Bangladesh, a thick paste which is made up of a mixture of butter or oil and carbon soot (obtained either from butter or mustard oil) called "Kajal" has been used since time immemorial to prevent ocular infection. This paste was used as an eyeliner on the conjunctival margin of the eyes and had both cosmetic and antimicrobial effects. Herein, we are likely to propose a mechanism of the microbicidal effect of "Kajal." Tears with their washing property facilitate the accumulation of microbes on the conjunctival margin of the eyes where "Kajal" in the form of a thick line was present. The synergistic effect of lysozymes (present in tears), individual antimicrobial property of butter or oil, and carbon particles present in "Kajal" finally resulted in the killing of infectious microbes without harming the surrounding cells or tissues. Moreover, oil or ghee as an ingredient of "Kajal" also helps in holding CNPs within the paste and does not allow their washing-off from the eyelines. This further increased the contact time between CNPs and microbes and resulted in an enhanced bactericidal effect of CNPs.

Multiple-drug-resistant (MDR) bacterial strains-mediated infections have increased the cases of mortality and morbidity worldwide. Since the arrival of this problem, microbiologists have been searching for biocompatible, low-cost, and effective bactericidal agents of natural origin [62]. There are certain features that make an antimicrobial agent an ideal one which includes specific properties like a) potential to obliterate or obstruct the growth of targeted microorganism; b) selective toxicity towards the targeted microorganism with no or minimal damage to surrounding cells and tissues; c) high stability, availability, and solubility in body fluids, and d) cost-effectiveness [24,63]. Our synthesized CNPs (CDs and carbon nanospheres) showed remarkable bactericidal potential against various pathogenic bacterial strains. Different studies demonstrated the concentration-dependent toxicity behavior of different types of carbon nanomaterials like carbon black or buckyballs, MWCNTs, and SWCNTs [64–66]. Recently, Singh *et al.* [1] using trypan-blue exclusion and propidium iodide uptake assays demonstrated that, in the presence of different concentrations of CNPs (200–500 µg/ml), 90.66%–95.7% of viable cells were observed in the solution. Moreover, in the same study, it was also claimed that, in the abovementioned concentration range of CNPs, no significant genotoxic or cytotoxic effect was observed on V-79 cell lines. Our synthesized CNPs were found both stable and soluble in water. These properties could be improved further with the help of various functional groups, chemical moieties, or different metallic NPs *via* covalent modifications, electrostatic interactions, hydrogen bonding, etc. as per laboratory requirements. For example, silver and zinc-based carbon nanocomposites showed remarkable and enhanced bactericidal effects against methicillin-resistant *S. aureus*, *Burkholderia cepacia*, *K. pneumoniae*, and *E. coli* bacteria [62,67–70]. Recently, spermidine-coated carbon quantum dots mediated killing of *S. aureus,* and *E. coli* was found to have MIC values tenfold lower than that of AgNPs [71]. Furthermore, the method of production of CNPs in the present research is ecofriendly, highly reproducible and cost-effective, and free of any metallic contamination. Overall, due to various novel properties like excellent water dispersibility, biocompatibility, easy and convenient surface modifications, and chemical inertness, these CNPs have tremendous applications in various fields of biotechnology [72], environment, pharmacology, and diagnostics [73], and nanosensors [74] and also as potential antibacterial agents.

4. CONCLUSION

In this study, we demonstrated the remarkable bactericidal potential of CNPs (CDs and carbon nanospheres) prepared from the soot of mustard oil and cow's clarified butter using the agar-well diffusion and XTT-colorimetric methods. The method of preparation of CNPs was cost-effective, highly reproducible, and ecofriendly. These prepared CNPs can be used as potential bactericidal agents alone or in combination with other substances like antibiotics, phytochemicals, metallic NPs, etc. against various pathogenic bacterial strains and on superficial infections like wounds and burns. Hence, they hold considerable promise for overcoming the limitations of antibiotics-mediated therapy like the evolution of MDR strains, which will lessen the financial and health burden globally. Moreover, as these CNPs are devoid of any metallic contaminations, they can be used as a promising agent in various other applications like bioimaging, labeling, nanosensors, probing, and diagnostics.

REFERENCES

1. Singh S, Singh D, Singh SP, Pandey AK. Candle soot derived carbon nanoparticles: assessment of physico-chemical properties, cytotoxicity and genotoxicity. Chemosphere 2019;214:130–5.
2. Ashfaq M, Verma N, Khan S. Highly effective Cu/Zn-carbon micro/nanofiber-polymer nanocomposite-based wound dressing biomaterial against the *Pseudomonas aeruginosa* multi- and extensively drug-resistant strains. Mater Sci Eng C 2017;77:630–41.
3. Tripathi KM, Sachan A, Castro M, Choudhary V, Sonkar SK, Feller JF. Green carbon nanostructured quantum resistive sensors to detect volatile biomarkers. Sustain Mater Technol 2018;16:1–11.
4. Coleman BR, Knight T, Gies V, Jakubek ZJ, Zou S. Manipulation and quantification of graphene oxide flake size: photoluminescence and cytotoxicity. ACS Appl Mater Interfaces 2017;9:28911–921.
5. Khare P, Singh A, Verma S, Bhati A, Sonker AK, Tripathi KM, *et al.* Sunlight-induced selective photocatalytic degradation of methylene blue in bacterial culture by pollutant soot derived nontoxic graphene nanosheets. ACS Sustain Chem Eng 2018;6:579–89.
6. Pankaj A, Tewari K, Singh S, Singh SP. Waste candle soot derived nitrogen doped carbon dots based fluorescent sensor probe: an efficient and inexpensive route to determine Hg(II) and Fe(III) from water. J Environ Chem Eng 2018;6:5561–9.
7. Sharma A, Das J. Small molecules derived carbon dots: synthesis and applications in sensing, catalysis, imaging, and biomedicine. J Nanobiotech 2019;17(1):92.
8. Zulfajri M, Abdelhamid HN, Sudewi S, Dayalan S, Rasool A, Habib A, *et al.* Plant part-derived carbon dots for biosensing. Biosensors (Basel) 2020;10(6):68.
9. Dong X, Bond AE, Pan N, Coleman M, Tang Y, Sun YP, *et al.* Synergistic photoactivated antimicrobial effects of carbon dots combined with dye photosensitizers. Int J Nanomedicine 2018;13:8025–35.
10. Jijie R, Barras A, Bouckaert J, Dumitrascu N, Szunerits S, Boukherroub R. Enhanced antibacterial activity of carbon dots functionalized with ampicillin combined with visible light triggered photodynamic effects. Colloids Surf B Biointerfaces 2018;170:347–54.
11. Tejwan N, Saha SK, Das J. Multifaceted applications of green carbon dots synthesized from renewable sources. Adv Colloid Interface Sci 2020;275:102046.
12. Lin X, Su J, Lin H, Sun X, Liu B, Kankala RK, *et al.* Luminescent carbon nanodots based aptasensors for rapid detection of kanamycin residue. Talanta 2019;202:452–59.
13. Lu S, Wu D, Li G, Lv Z, Chen L, Chen Z, *et al.* Carbon dots-based ratio metric nanosensor for highly sensitive and selective detection of mercury(II) ions and glutathione. RSC Adv 2016;6(105):103169–77.
14. Wang Y, Zhu Y, Yu S, Jiang C. Fluorescent carbon dots: rational synthesis, tunable optical properties, and analytical applications. RSC Adv 2017;7(65):40973–89.
15. Roshni V, Misra S, Santra S, Divya O. One pot green synthesis of C-dots from groundnuts and its application as Cr(VI) sensor and in vitro bioimaging agent. J Photochem 2018;375:28–36.
16. Wang L, Yuan Z, Karahan HE, Wang Y, Sui X, Liu F, Chen Y. Nanocarbon materials in water disinfection: state-of-the-art and future directions. Nanoscale 2019;11(20):9819–39.
17. Yan F, Jiang Y, Sun X, Bai Z, Zhang Y, Zhou X. Surface modification and chemical functionalization of carbon dots: a review. Mikrochim Acta 2018;185(9):424.
18. Mohammed MKA, Duha SA, Mohammad RM. Studying antimicrobial activity of carbon nanotubes decorated with metal-doped ZnO hybrid materials. Mater Res Express 2019;6:055404; http://doi.org/10.1088/2053-1591/ab0687

19. Rahman G, Najaf Z, Mehmood A, Bilal S, Shah AHA, Mian SA, *et al.* An overview of the recent progress in the synthesis and applications of carbon nanotubes. *C* J Carbon Res 2019;5:3.
20. Sun M, Qu A, Hao C, Wu X, Xu L, Xu C, *et al.* Chiral up conversion heterodimers for quantitative analysis and bioimaging of antibiotic-resistant bacteria *in vivo*. Adv Mater 2018;30(50):e1804241.
21. Cui F, Ye Y, Ping J, Sun X. Carbon dots: current advances in pathogenic bacteria monitoring and prospect applications. Biosens Bioelectron 2020;156:112085.
22. Jones K, Patel N, Levy M, Storeygard A, Balk D, Gittleman JL, *et al.* Global trends in emerging infectious diseases. Nature 2008;451**:**990–3; http://doi.org/10.1038/nature06536
23. Zhou J, Zhou H, Tang J, Deng S, Yan F, Li W, *et al.* Carbon dots doped with heteroatoms for fluorescent bioimaging: a review. Microchim Acta 2016;184:343–68.
24. Lakshmi SD, Pramod KA, Gurumurthy H. Activated carbon nanoparticles from biowaste as new generation antimicrobial agents: a review. Nano-Struct Nano-Objects 2018;16:306–21.
25. Kumar R, Kumar VB, Gedanken A. Sonochemical synthesis of carbon dots, mechanism, effect of parameters, and catalytic, energy, biomedical and tissue engineering applications. Ultrason Sonochem 2020;64:105009.
26. Khare C. *Brassica campestris* Linn. var. rapa (L.) Hartm. In: Khare C (ed.). Indian medicinal plants, Springer, New York, NY, 2007; http://doi.org/10.1007/978-0-387-70638-2_236
27. Agrawal MK, Rathore D, Goyal S, Varma A, Varma A. Antibacterial efficacy of *Brassica campestris* root, stem and leaves extracts. Int J Adv Res 2013;5:131–5.
28. Kaushik R, Jain J, Rai P. Therapeutic potentials of cow derived products- a review. Int J Pharm Sci Res 2016;7(4):1383–90.
29. Khameneh B, Iranshahy M, Soheili V. Review on plant antimicrobials: a mechanistic viewpoint. Antimicrob Resist Infect Control 2019;8:118; http://doi.org/10.1186/s13756-019-0559-6
30. Joshi DR, Nisha Adhikari. Benefit of cow urine, milk, ghee, curd, and dung versus cow meat. Acta Sci Pharm Sci 2019;3.8:169–75.
31. Sindhuja S, Prakruthi M, Manasa R, Naik R S, Shivananjappa M. Health benefits of ghee (clarified butter) – a review from ayurvedic perspective. IP J Nutr Metab Health Sci 2020;3(3):64–72.
32. Hamouda RA, Hussein MH, Abo-Elmagd RA, Bawazir SS. Synthesis and biological characterization of silver nanoparticles derived from the cyanobacterium *Oscillatoria limnetica*. Sci Rep 2019;9(1):13071; http://doi.org/10.1038/s41598-019-49444-y
33. Al-Bakri GA, Afifi FU. Evaluation of antimicrobial activity of selected plant extracts by rapid XTT colorimetry and bacterial enumeration. J Microbiol Meth 2007;68:19–25.
34. Pahal V, Kaur A, Dadhich KS. Effect of combination therapy using cow (*Bos indicus*) urine distillate and some indian medicinal plants against selective pathogenic gram-negative bacteria. Int J Pharm Sci Res 2017;8(5):2134–42.
35. Shikha S, Chaudhuri SR, Bhattacharyya MS. Facile one pot greener synthesis of sophorolipid capped gold nanoparticles and its antimicrobial activity having special efficacy against Gram Negative *Vibrio cholerae*. Sci Rep 2020;10(1):1463; http://doi.org/10.1038/s41598-019-57399-3
36. Ray SC, Sagha A, Jana NR, Sarkar R. Fluorescent carbon nanoparticles: synthesis, characterization, and bioimaging application. J Phys Chem C 2009;43:18546–51.
37. Lehrer RI, Rosenman M. Ultrasensitive assays for endogenous antimicrobial polypeptides. J Microbiol Meth 1991;137:167–73.
38. Dhandapani K, Venugopal K, Kumar JV. Ecofriendly and green synthesis of carbon nanoparticles from rice bran: characterization and identification using image processing technique. Int J Plast Technol 2019;23:56–66; http://doi.org/10.1007/s12588-019-09240-9
39. Roshni V, Gujar V, Pathan H, Islam S, Tawre M, Pardesi K, *et al.* Bioimaging applications of carbon dots (C. dots) and its cystamine functionalization for the sensitive detection of Cr(VI) in aqueous samples. J Fluoresc 2019;29(6):1381–92.
40. Zhao C, Wang X, Wu L, Wu W, Zheng Y, Lin L, *et al.* Nitrogen-doped carbon quantum dots as an antimicrobial agent against *Staphylococcus* for the treatment of infected wounds. Colloids Surf B Biointerfaces 2019;179:17–27.
41. Gao Z, Yang D, Wan Y, Yang Y. One-step synthesis of carbon dots for selective bacterial inactivation and bacterial differentiation. Anal Bioanal Chem 2020;412(4):871–80.
42. Shah SM, Rezaei B, Ensafi AA, Etemadifar Z. An ancient plant for the synthesis of a novel carbon dot and its applications as an antibacterial agent and probe for sensing of an anti-cancer drug. Mater Sci Eng C Mater Biol Appl 2019;98:826–33.
43. Singh SS, Bairagi PK, Verma N. Candle soot-derived carbon nanoparticles: an inexpensive and efficient electrode for microbial fuel cells. Electrochimica Acta 2018;264:119–27.
44. Rajeshwari P, Dey TK. Novel HDPE nanocomposites containing aluminum nitride (nano) particles: micro-structural and nano-mechanical properties correlation. Mater Chem Phys 2017;190:175–86.
45. Mohanty B, Verma AK, Claesson P, Bohidar HB. Physical and anti-microbial characteristics of carbon nanoparticles prepared from lamp soot. Nanotechnology 2007;18:445102.
46. Prasad KS, Chuang MC, Ho JA. Synthesis, characterization, and electrochemical applications of carbon nanoparticles derived from castor oil soot. Talanta 2012;188:445–9.
47. Dong X, Liang W, Meziani MJ, Sun YP, Yang L. Carbon dots as potent antimicrobial agents. Theranostics 2020;10(2):671–86.
48. Yang C, Mamouni J, Tang Y, Yang L. Antimicrobial activity of single-walled carbon nanotubes: length effect. Langmuir 2010;26(20):16013–9.
49. Mocan T, Matea CT, Pop T, Mosteanu O, Buzoianu AD, Suciu S, *et al.* Carbon nanotubes as anti-bacterial agents. Cell Mol Life Sci 2017;74(19):3467–79.
50. Liu S, Wei L, Hao L, Fang N, Chang MW, Xu R, *et al.* Sharper and faster ‘‘nano darts’’ kill more bacteria: a study of antibacterial activity of individually dispersed pristine single-walled carbon nanotube. ACS Nano 2009;3:3891–02.
51. Varghese S, Kuriakose S, Jose S. Antimicrobial activity of carbon nanoparticles isolated from natural sources against pathogenic Gram-Negative and Gram-Positive bacteria. J Nanosci 2013; Article ID 457865:1–5; http://doi.org/10.1155/2013/457865
52. Aloysius C, Varghese AA, Pattekkal Ali S, Sukirtha TH, Aloysius Sabu N, Cyriac J, *et al.* Antibacterial activity of carbon nanoparticles isolated from chimney soot. IET Nanobiotechnol 2019;13(3):316–9.
53. Su S, Shelton CB, Qiu J. Proceedings of the ASME 2013 International Mechanical Engineering Congress and Exposition November 15-21, 2013, San Diego, CA, 2013.
54. Anand A, Unnikrishnan B, Wei SC, Chou CP, Zhang LZ, Huang CC. Graphene oxide and carbon dots as broad-spectrum antimicrobial agents - a minireview. Nanoscale Horiz 2019;4(1):117–37.
55. Jiang YW, Gao G, Zhang X, Jia HR, Wu FG. Antimicrobial carbon nanospheres. Nanoscale 2017;9(41):15786–95.
56. Zare-Zardini H, Ahmad A, Mehdi S, Ahmad A. Studying of antifungal activity of functionalized multiwalled carbon nanotubes by microwave-assisted technique.Surf Interface Anal 2012;3:1–5; http://doi.org/10.1002/sia.5152
57. Simmons TJ, Lee SH, Park TJ, Hashim DP, Ajayan PM, Linhardt RJ. Antiseptic single wall carbon nanotube bandages. Carbon 2009;47:1561–4.
58. Amiri A, Zardini HZ, Shanbedi M, Maghrebi M, Baniadam MBT. Efficient method for functionalization of carbon nanotubes by lysine and improved antimicrobial activity and water-dispersion. Mater Lett 2012;72:153–6.
59. Arias LR, Yang L. Inactivation of bacterial pathogens by carbon nanotubes in suspensions. Langmuir 2009;25:3003–12.
60. CDC, 2019. Available via https://www.cdc.gov/DrugResistance/Biggest-Threats.html

61. Chen J, Andler SM, Goddard JM, Nugen SR, Rotello VM. Integrating recognition elements with nanomaterials for bacteria sensing. Chem Soc Rev 2017;46(5):1272–83.
62. Dizaj SM, Mennati A, Jafari S, Khezri K, Adibkia K. Antimicrobial activity of carbon-based nanoparticles. Adv Pharm Bull 2015;5:19–23.
63. Rennie PR. Current and future challenges in the development of antimicrobial agents. Springer-Verlag, Berlin, Germany, pp 45–65, 2012; http://doi.org/10.1007/978-3-642-28951-4
64. Arora S, Kaur H, Kumar R, Kaur R, Rana D, Rayat CS, *et al. In vitro* cytotoxicity of multiwalled and single walled carbon nanotubes on human cell lines. Fullerene Nanotubes Carbon Nanostruct 2015;23:377–82.
65. Mehta VN, Jha S, Basu H, Singhal RK, Kailasa SK. One step hydrothermal approach to fabricate carbon dots from apple juice for imaging of mycobacterium and fungal cells. Sensors Actuators B Chem 2015;213:434–43.
66. Kasibabu BSB, D'souza SL, Jha S, Singhal RK, Basu H, Kailasa SK. One-step synthesis of fluorescent carbon dots for imaging bacterial and fungal cells. Anal Methods 2015;7:2373–8.
67. Leid J, Ditto A, Knapp A, Shah P, Wright B, Blust R. *In vitro* antimicrobial studies of silver carbine complexes: activity of free and nanoparticle carbene formulations against clinical isolates of pathogenic bacteria. J Antimicrob Chemother 2012;67:138–48.
68. Dong X, Awak MA, Tomlinson N, Tang Y, Sun YP, Yang L. Antibacterial effects of carbon dots in combination with other antimicrobial reagents. PLoS One 2017;12(9):e0185324.
69. Prasad K, Lekshmi G, Ostrikov K, Lussini V, Blinco J, Mohandas M, *et al.* Synergic bactericidal effects of reduced graphene oxide and silver nanoparticles against Gram-positive and Gram-negative bacteria. Sci Rep 2017; Available via https://www.ncbi.nlm.nih.gov/pmc/articles/PMC5431540/
70. Ardekani SM, Dehghani A, Ye P, Nguyen KA, Gomes VG. Conjugated carbon quantum dots: potent nano-antibiotic for intracellular pathogens. J Colloid Interface Sci 2019;552:378–87.
71. Harroun SG, Lai JY, Huang CC, Tsai SK, Lin HJ. Reborn from the Ashes: turning organic molecules to antimicrobial carbon quantum dots. ACS Infect Dis 2017;3(11):777–9.
72. Tejwan N, Saini AK, Sharma A, Singh TA, Kumar N, Das J. Metal-doped and hybrid carbon dots: a comprehensive review on their synthesis and biomedical applications. J Control Release 2021;10(330):132–50.
73. Dugam S, Nangare S, Patil P, Jadhav N. Carbon dots: a novel trend in pharmaceutical applications. Ann Pharm Fr 2021;79(4):335–45.
74. Guo FN, Wang YT, Wu N, Feng LX, Zhang HC, Yang T, *et al.* Carbon nitride nanoparticles as ultrasensitive fluorescent probes for the detection of α-glucosidase activity and inhibitor screening. Analyst 2021;7(3):1016–22.

How to cite this article:
Pahal V, Kumar P, Kumar R, Kumar P, Kumar V. Characterization and comparative assessment of bactericidal activity of carbon nanodots (CDs) and nanoparticles (CNPs) prepared from soot's of clarified butter and mustard oil, respectively. J Appl Biol Biotech 2023;11(6):233-248.
Doi: 10.7324/JABB.2023.115277